15.4 MESOSCALE ENVIRONMENT ASSOCIATED WITH MEDITERRANEAN HEAVY PRECIPITATING EVENTS

Didier Ricard*, Véronique Ducrocq, Raphaël Bresson, and Ludovic Auger
CNRM/GAME (Météo-France, CNRS), Toulouse, France

1. INTRODUCTION

The Mediterranean region is regularly affected by heavy precipitating events (HPEs) potentially associated with devastating flash floods. The southern France is particularly prone to this risk. Indeed, the configuration of this area is propitious for triggering these HPEs. The Mediterranean sea acts as a vast heat and moisture reservoir from which these systems pump their energy. Moreover, the steep orography of this area (Massif Central, Pyrenees, South Alps) induces low-level convergence and favours upward motion.

In the course of these last years, the flagship case is without doubt the paroxysmal Gard flooding in 8-9 September 2002 that produced more than 600 mm in 24 hours (Delrieu et al., 2005). Using high-resolution simulations, Nuissier et al. (2007) and Ducrocq et al. (2007) have studied the synoptic and mesoscale features associated with this mesoscale convective system. This flooding disaster caused 24 casualties and more than 1.2 billions euros damages. Without reaching this destructive level, many other severe HPEs occurred over this area during the last years.

In this study, first, the mesoscale environment in which these systems grow is characterized for a set of past events that have affected southern France. Then, idealized high-resolution simulations are carried out to assess the sensitivity to the mesoscale environment features of the triggering and evolution of the heavy precipitating systems.

2. HPES DATABASE

As a first step a database of HPEs has been elaborated. We select the precipitating systems with daily precipitation more than 150 mm that occurred over southern France between the 1 August and 31 December for a 5-year period (2002-2006). We focus on this period because the HPEs mostly occur during autumn. Hourly raingauges and lightning data are used to examine the life cycle of each event and determine its different phases (formative, mature and dissipating stages). For the heaviest precipitation events ($\geq$ 200 mm/day), the mature stage occurs more frequently in the morning and the dissipation stage in the first part of the night. The mean duration is about 29 hours (ranging from 13 to 58 hours). Compared to the climatology over a 40-yr period (1967-2006) (Fig. 1a), the monthly distribution for the five studied years (2002-2006) (Fig.1b) highlights also a peak of occurrence for HPEs ($\geq$150 mm/day) in October.

Table 1 shows the number of precipitating events with daily precipitation larger than 150 mm and 200 mm for the 5-yr recent period compared to the 40-yr period. Over the 2002-2006 period, there are 23 days [50 days] with daily precipitation larger than 200 mm [to 150 mm]. There is a great interannual variability with an annual mean of about 4 days above 200 mm and 10 days above 150 mm. Indeed, the year 2003 totals the larger number of cases, contrary to the year 2004 that totals the weakest number. There is an increase of the number of HPEs for the 5 last years compared to the entire 40-yr period.

3. MESOSCALE ANALYSES

In order to characterize the mesocale environment associated with each HPE, 3D-Var mesoscale analyses based on the VARPACK ALADIN (Auger, 2005) at a 10-km resolution are performed for each HPE. The background is provided by a 6-hour ALADIN forecast. The analysed data are surface mesonet over France (2m temperature and relative humidity, 10m winds), synop, buoy and ship data, AMDAR-ACAR aircraft observations, wind profilers observations, radiosoundings and satellite data (QuikSCAT and SEVERI from 2005). In comparison with mesocale analysis based on optimal interpolation (Calas et al., 2000), 3D-Var analysis is multivariate and enables to take into account a higher number of observations. These reanalyses are realized every six hours during the full life cycle of HPEs.

4. COMPOSITE ANALYSES

To have a big picture of the conditions that prevail during these events, we performed composite analyses following Moore et al. (2003), Rudari et al. (2004) or Schumacher and Johnson (2005) by averaging different parameters during the different stages for all HPEs.

The composite analyses for the 40 HPEs over the 2002-2006 period for formative, mature and dissipating stages (Fig. 2) show that HPEs are associated with a trough-ridge pattern which induces a southwesterly

* *Corresponding author address:* Didier Ricard, Météo-France, CNRM/GMME/Micado, 31 057 Toulouse cedex 1, France; e-mail: didier.ricard@meteo.fr.

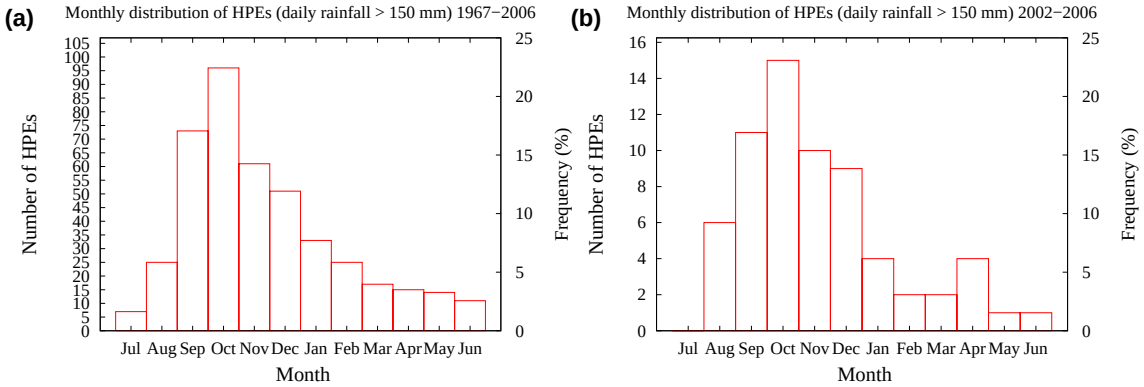

Figure 1: Monthly distribution of precipitating events with daily rainfall larger than 150 mm over 1967-2006 (left) and over 2002-2006 (right).

Table 1: Yearly distribution of days with daily rainfall larger than 150 mm or 200 mm (between 15 August and 31 December), the distribution (and mean) over 2002-2006 and 1967-2006 periods is also displayed.

Daily rainfall	**2002**	**2003**	**2004**	**2005**	**2006**	**2002-2006 (mean)**	**1967-2006 (mean)**
$\geq$ **150 mm**	8	15	5	9	13	50 (10)	305 (7.6)
$\geq$ **200 mm**	3	8	2	5	5	23 (4.6)	149 (3.7)

flow in mid-troposphere over southern France. During the mature phase, this flow is diffluent over France, which favours the ascending motion. The synoptic conditions evolve quite slowly with a shift eastward. Precipitable water (PW) is higher along the coast at foothills of Cévennes (southeast side of the Massif Central) and South Alps, at the entrance of the Rhône Valley and upstream over the Mediterranean sea. There is also an area of strong instability upstream over sea. The southerly low-level jet brings moisture and energy northward. The most intense moisture flux comes from the Mediterranean sea and rushes into the Rhône Valley (between the Massif Central and the Alps). Then, in function of the location of heavy rainfall, four domains are considered: Languedoc-Roussillon (LR), Cévennes-Vivarais (CV), South Alps (SA) and Corsica (C) areas (see Fig. 3 for location of the domains). Composite analyses are also performed for each domain (Fig. 3) and described in the following.

4.1 *Cévennes-Vivarais area*

Only the HPEs that affected the CV area (blue box in Fig. 3d) are considered, the synoptic pattern is quite similar to the complete 40-HPEs composite with a trough-ridge configuration. Figure 3g shows that the humidity flux is stronger than for the complete composite (Fig. 2h) due to higher values of humidity. The southerly low-level jet has a slight east component when reaching land. Strong moisture convergence (MOCON) takes place along the foothills of the Cévennes favouring the triggering of precipitating cells.

4.2 *South Alps area*

For HPEs occurring over the SA area (red box in Fig. 3e), the synoptic conditions also reveal a trough-ridge configuration but shifted eastward inducing a southwesterly flow over the target area where heavy precipitation occured. The moisture flux is more intense due to a faster low-level jet ($\geq$ 15 m/s). The orientation of the low-level jet is also different: it has a southwesterly orientation from Mediterranean Sea towards the South Alps and the Gulf of Genoa. The strip of high PW streches from the Mediterranean Sea to the Gulf of Genoa with higher values at the foothills of the Alps.

4.3 *Languedoc-Roussillon area*

For HPEs occurring over the Languedoc-Roussillon area (green box in Fig. 3f), there is an accentued upper-level geopotential low over Spain that induces a southeasterly flow over the target area. A surface low is also present over Balearic islands. The low-level jet has a southeasterly orientation with high values of MOCON and moisture flux along the Languedoc-Roussillon coast and high values of CAPE offshore.

4.4 *Corsica area*

For HPEs occurring over the Corsica area, the synoptic conditions are similar to the previous ones. They induces a southwesterly over the target area. The low-level jet has a southerly orientation with a slight east component with high value of CAPE upstream offshore. There are also high values of MOCON along the east side of Corsica (not shown).

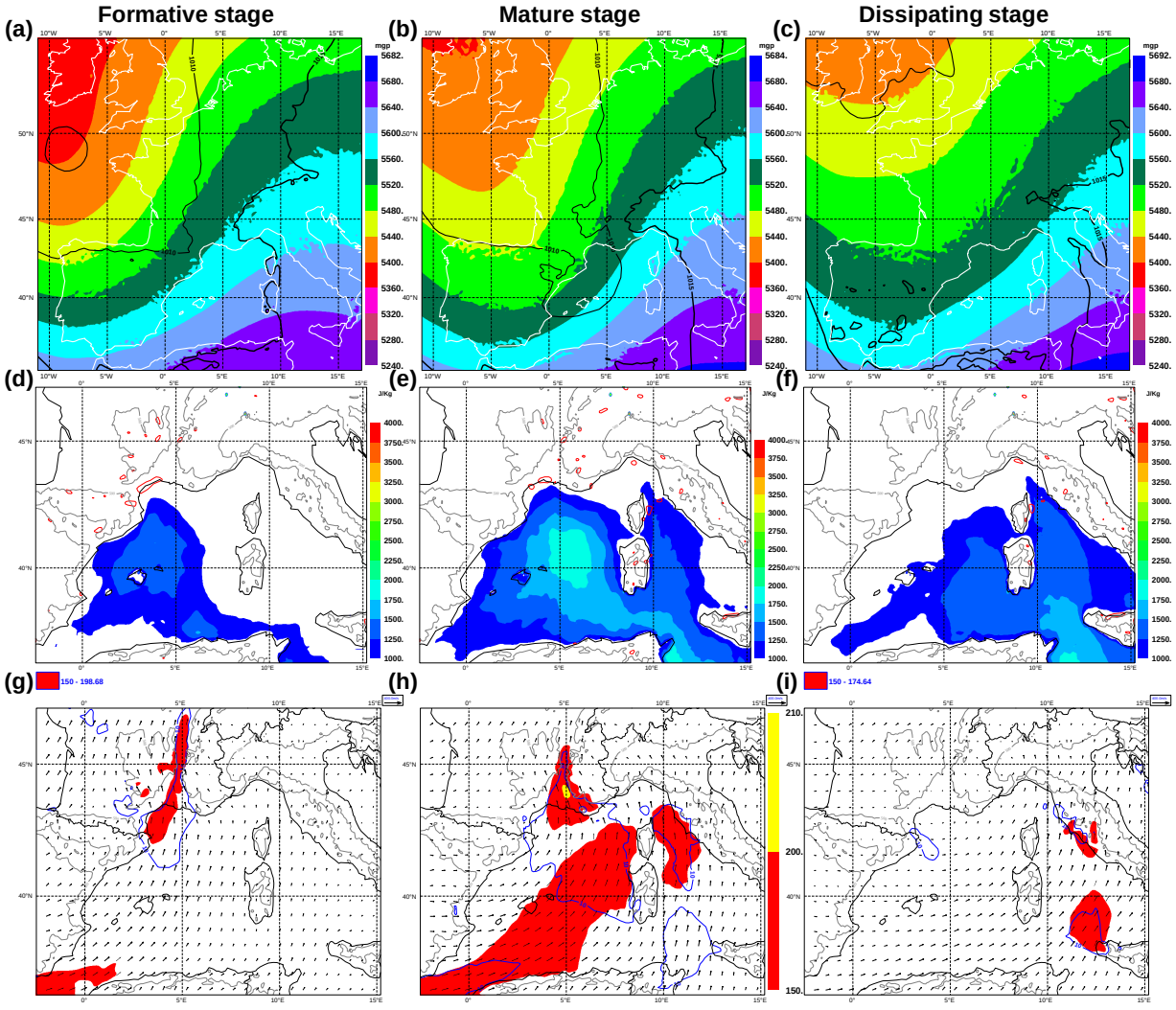

Figure 2: Composite analysis for all HPEs over 2002-2006 (40 cases) during formative (left column), mature (middle column) and dissipating stages (right column): geopotential heights (color scale, every 40 mgp) and surface pressure (hPa, black lines) (top panels), CAPE (color scale, every 250 J/Kg), precipitable water (contours every 1 mm above 30 mm; blue lines) and moisture flux convergence (contours every 1E-6 s-1; red lines) (middle panels), 1000-700 hPa integrated moisture flux (arrows and color scale, every 50 Kg/m/s), 925 hPa wind speed (contours every 5 m/s above 10 m/s; blue lines) (bottom panels).

4.5 *HPEs with daily precipitation above 200mm*

If we consider the heaviest PEs (more than 200 mm/day), composite analyses show that the available instability is higher and the amount of water vapour along the French coast is larger. Indeed, this higher moisture is brought by more intense low-level jets (not shown).

5. IDEALIZED NUMERICAL SIMULATIONS

To further investigate the role of the different ingredients identified with mesoscale analyses, idealized simulations are carried out. In particular, the structure of the moist low-level jet that impinges the relief is studied. Based on idealized simulations, Chen and Lin (2005) identified four moist flow regimes for a conditionaly unstable flow over an isolated mountain ridge. In this study, high resolution simulations (2.5 km) are performed with the research model MESO-NH (Lafore et al., 1998) for an idealized convective flow but using a real topography (as in Gheusi and Stein, 2003). The model is centered over North-Western Mediterranean regions. Initial and boundary conditions for temperature and humidity are derived from the sounding of Nîmes at 12 UTC, 8 September 2002 (Gard flood) (Fig. 4). A unidirectional southeasterly wind U is imposed through the whole depth of the atmosphere. In the low levels (below 3000 m) the strong wind is focused on a 100 km wide band in order to represent a low-level jet, the band has a southeast-northwest orientation. The effects of the low-level humidity distribution, instability and speed of flow are investigated through sensitivity tests. Table 2 lists the characteristics of the simulations.

5.1 *Reference simulation*

For the reference simulation MDGHU, high values of humidity are focused into the low-level jet (Fig 5a). Quasi-stationarity is reached within a few hours, a

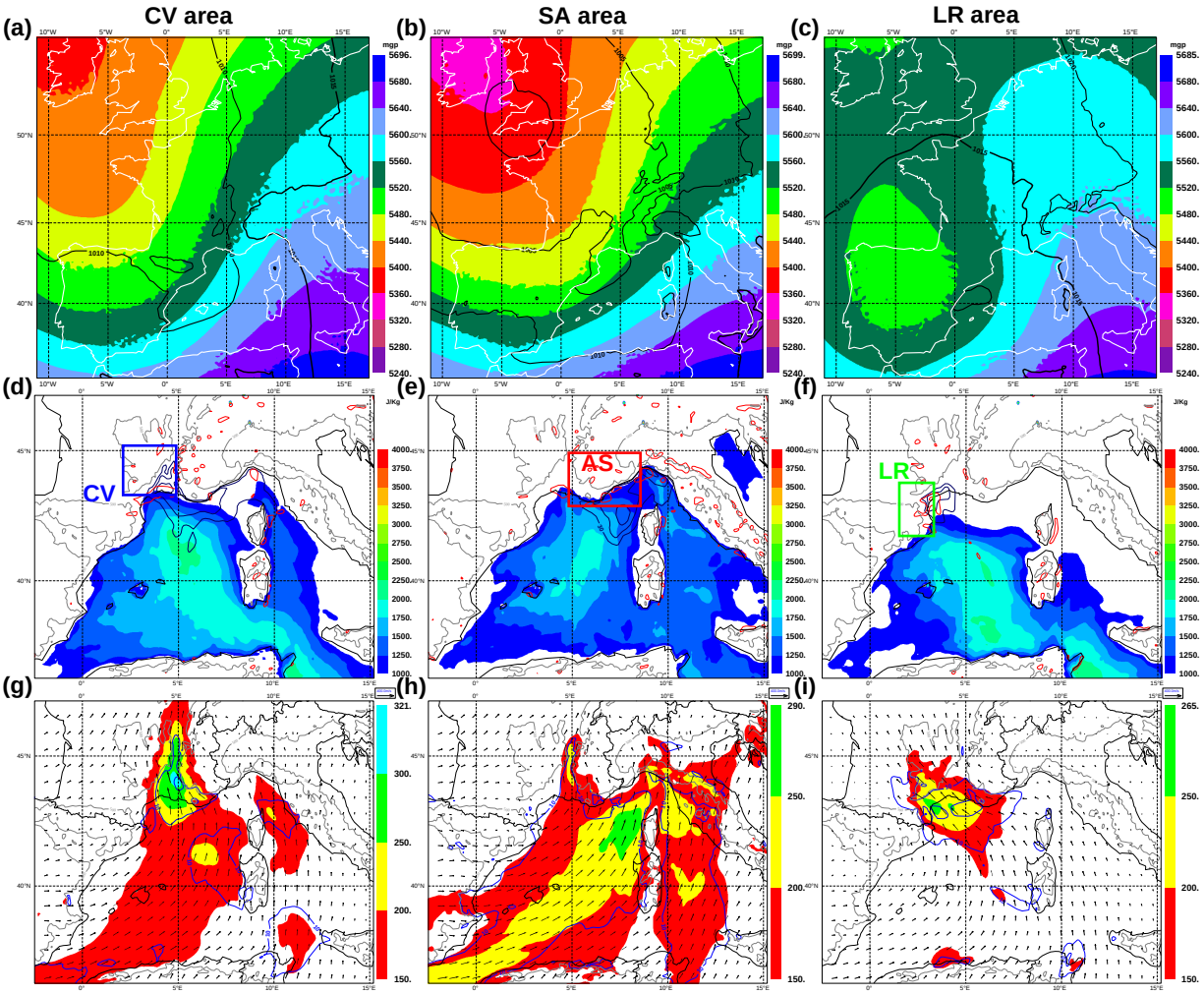

Figure 3: Composite analysis over 2002-2006 during the mature stage for HPEs that occured over CV area (left column), SA area (middle column), and LR area (right column): geopotential heights (color scale, every 40 mgp) and surface pressure (hPa, black lines) (top panels), CAPE (color scale, every 250 J/Kg), precipitable water (contours every 1 mm above 30 mm, blue lines) and surface moisture flux convergence (contours every 1E-6 s-1, red lines) (middle panels), 1000-700 hPa integrated moisture flux (arrows and color scale, every 50 Kg/m/s), 925 hPa wind speed (contours every 5 m/s above 10 m/s, blue lines) (bottom panels). The location of the three areas are indicated by the boxes (middle panels).

backbuilding convective system forms and precipitation area spreads from sea to Massif Central. Deflection of the flow by the Alps reinforces the low-level convergence. A cold pool forms under the system leaning againt the southeastern flank of Massif Central and spreading southward over sea (Fig. 5b). The moist and unstable low-level jet impinges the leading edge of the cold pool, the induced updrafts trigger convective cells. Backward trajectories and budgets on microphysical variables are used to investigate the formation of this cold pool. A part of precipitation is evaporated by the mid-tropospheric drier air, that generates cooling and downdrafts under the convective system.

5.2 *Impact of humidity distribution*

First, the sensitivity to the humidity distribution is tested with a uniform distribution (simulation UNIHU) and a stronger gradient (simulation STGHU). With a uniform high humidity, there is no cold pool (Fig. 6a). The convective system forms and stays over the relief of Massif Central, convective cells are triggerred by orographic forcing. With a large humidity focused into the jet and drier conditions out of the jet, an intense cold pool spreads southeastward (Fig. 6d). The leftward deflection of drier air by the Alps accentuates the low-level convergence at foothills of Massif Central. When focusing the humidity, the updrafts are stronger, which contribute to the formation of more hydrometeors. The precipitation drag is greater, the evaporative cooling and the strength of downdrafts are enhanced. When the distribution of humidity is high and uniform, less relative dry air is dragged by compensating downdrafts and the evaporative cooling is weaker.

5.3 *Impact of wind speed*

Then, the sensitivity to the speed of the low-level flow is examined with simulations WIN10 (slower flow) and WIN20 (faster flow). With a slower flow, the convec-

Table 2: Initial humidity, wind speed and CAPE of the initial sounding for all the experiments. 24h accumulated rain maximum and rain surface are also displayed after 24h simulation.

Simulations	humidity distribution	Wind speed U (m/s)	Initial CAPEMAX (J/kg)	24h precipitation max (mm)	rain surface (km^2)
MDGHU	high humidity focused into the jet	15	400	526	63556
UNIHU	high uniform humidity	15	400	419	76833
STGHU	as MDGHU but with drier conditions out of the jet	15	400	661	55400
WIN10	as MDGHU	10	400	460	67709
WIN20	as MDGHU	20	400	888	57652
LCAPE	as MDGHU	15	190	646	57439
MCAPE	as MDGHU	15	1000	523	71211
HCAPE	as MDGHU	15	2050	390	73152

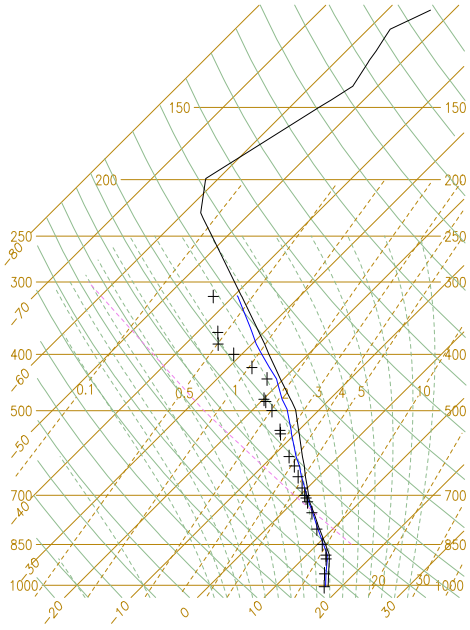

Figure 4: Sounding of Nîmes on 8 September 2002 at 12 UTC.

tive system is located upstream over sea. Upward forcing is located along the east leading edge of a strong cold pool (Fig. 6c). With a faster flow, the system is located downstream over the relief, there is no cold pool (Fig. 6b); lifting is favoured by orography. There is less deflection of the flow by the Alps. The speed of the flow impacts on the moisture feeding and thus modulates the precipitation quantity. Indeed, the strong flow induces a more intense low-level moiture flux with more precipitation. For the weak flow, the advection time is long enough for a cold pool to develop and thus more precipitation evaporates.

5.4 *Impact of instability*

Finally, the impact of instability is tested by modifying the low-level thermodynamic characteristics of the sounding. For simulation LCAPE, instability is decreased by a low-level drying to 92 % of humidity. For simulations MCAPE and HCAPE, instability is increased by a five-degree warming at the ground maintening a constant specific humidity for MCAPE and increasing relative humidity to 85 % for HCAPE. When decreasing instability, the system anchoring is similar to simulation WIN20 and the cold pool is very weak (Fig. 6e). On the contrary, when increasing instability, a strong cold pool spreads southward and between the reliefs of Massif Central and Alps (Fig. 6f).

6. CONCLUSION

To sum up, mesoscale composite analyses show that low-level moisture flux impinges the region where heavy rainfall occurs. Moisture and instability sources are located upstream and transported by low-level jets toward the target area. Moisture convergence is high just before reaching the target area and certainly helps with orographic forcing to trigger precipitating cells. Then, using idealized high-resolution simulations, it was found that the humidity distribution has an impact on the low-level convergence areas and on the location of the convective system. The cold pool strengh increases with a weaker flow and/or more instability. Increasing the instability results in higher total rain, spread over a larger area, leading to a weaker local maximum. Increasing the speed of the wind result in higher total rain focused over a smaller area and thus a higher local maximum (Tab. 2).

REFERENCES

Auger, L., 2005: Analysis of surface obervations. *15th ALADIN Workshop*, Bratislava, 6-10 June 2005.

Calas, C., V. Ducrocq, and S. Sénési, 2000: Mesoscale analyses and diagnostic parameters for deep convection nowcasting. *Meteorol. Appl.*, **7**, 145–161.

Chen, S.-H., and Y.-L. Lin, 2005: Effects of moist froude number and cape on a conditionally unstable flow over a mesoscale moutain ridge. *J. Atmos. Sci.*, **62**, 331–350.

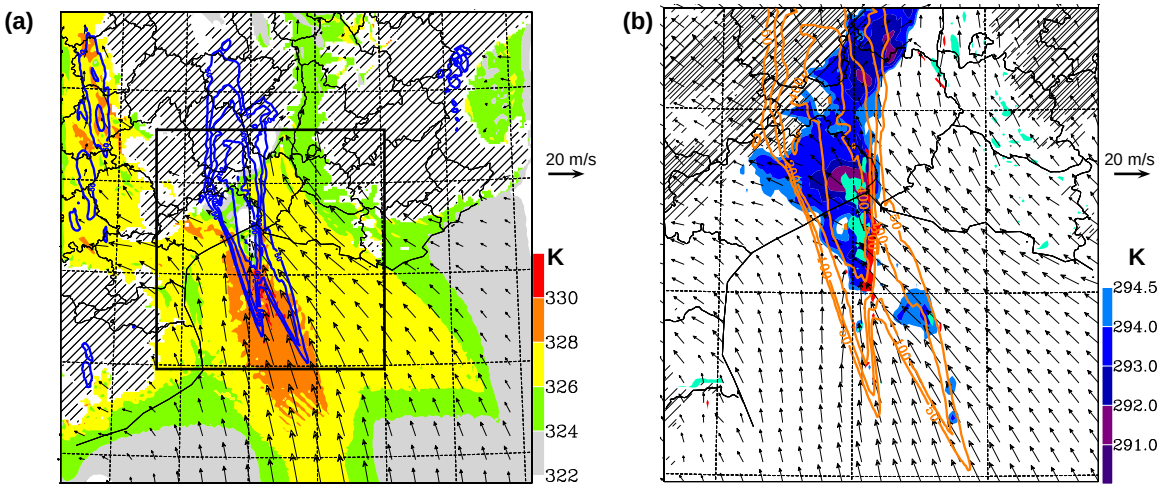

Figure 5: Reference simulation MDGHU 48h after the start of the simulation: a) θ_e at 500 m (color scale at right), 500-m ASL wind vectors and 24h accumulated precipitation (blue lines, 50, 100, 200, 400 and 600 mm) centered over southern France, b) θ_v on the first level of the model (color scale at right), 36-m AGL wind vectors, vertical velocity greater than 1 m/s (red areas) and lower than -0.5 m/s (green areas) at 600 m, 24h accumulated precipitation (orange lines, 50, 100, 200, 400 and 600 mm), zoomed over the black box. The relief is hatched above 500 m.

Delrieu, G., V. Ducrocq, É. Gaume, J. Nicol, O. Payrastre, E. Yates, P.-E. Kirstetter, H. Andrieu, P.-A. Ayral, C. Bouvier, J.-D. Creutin, M. Livet, S. Anquetin, M. Lang, L. Neppel, C. Obled, J. Parent du Châtelet, G.-M. Saulnier, A. Walpersdorf, and W. Wobrock, 2005: The catastrophic flash-flood event of 8–9 September 2002 in the Gard region, France: A first case study for the Cévennes-Vivarais Mediterranean Hydrometeorological Observatory. *J. Hydrometeor.*, **6**, 34–52.

Ducrocq, V., O. Nuissier, D. Ricard, C. Lebeaupin, and T. Thouvenin, 2007: A numerical study of three catastrophic precipitating events over western mediterranean region (southern france). part ii: Mesoscale triggering and stationarity factors. *Quart. J. Roy. Meteor. Soc.*

Gheusi, F., and J. Stein, 2003: Small-scale rainfall mechanisms for an idealized convective southerly flow over the Alps. *Quart. J. Roy. Meteor. Soc.*, **129**, 1819–1840.

Lafore, J.-P., J. Stein, N. Asencio, P. Bougeault, V. Ducrocq, J. Duron, C. Fischer, P. Héreil, P. Mascart, V. Masson, J.-P. Pinty, J.-L. Redelsperger, É. Richard, and J. Vilà-Guerau de Arellano, 1998: The Meso-NH Atmospheric Simulation System. Part I: Adiabatic formulation and control simulations. Scientific objectives and experimental design. *Ann. Geophysic.*, **16**, 90–109.

Moore, J. T., F. H. Glass, C. E. Graves, S. M. Rochette, and M. J. Singer, 2003: The environment of warm-season elavated thunderstorms associated with heavu rainfall over the Central United States . *Wea. Forecasting*, **18**, 861–878.

Nuissier, O., V. Ducrocq, D. Ricard, C. Lebeaupin, and S. Anquetin, 2007: A numerical study of three catastrophic precipitating events over Western Mediterranean region (Southern France). Part I: Numerical framework and synoptic ingredients. *Quart. J. Roy. Meteor. Soc.*

Rudari, R., D. Entekhabi, and G. Roth, 2004: Terrain and multiple-scale interaction as factors in generating extreme precipitation events. *J. Hydrometeor.*, **5**, 390–404.

Schumacher, R. S., and R. H. Johnson, 2005: Organization and environmental properties of extreme-rain-producing mesoscale convective systems. *Mon. Wea. Rev.*, **133**, 961–976.

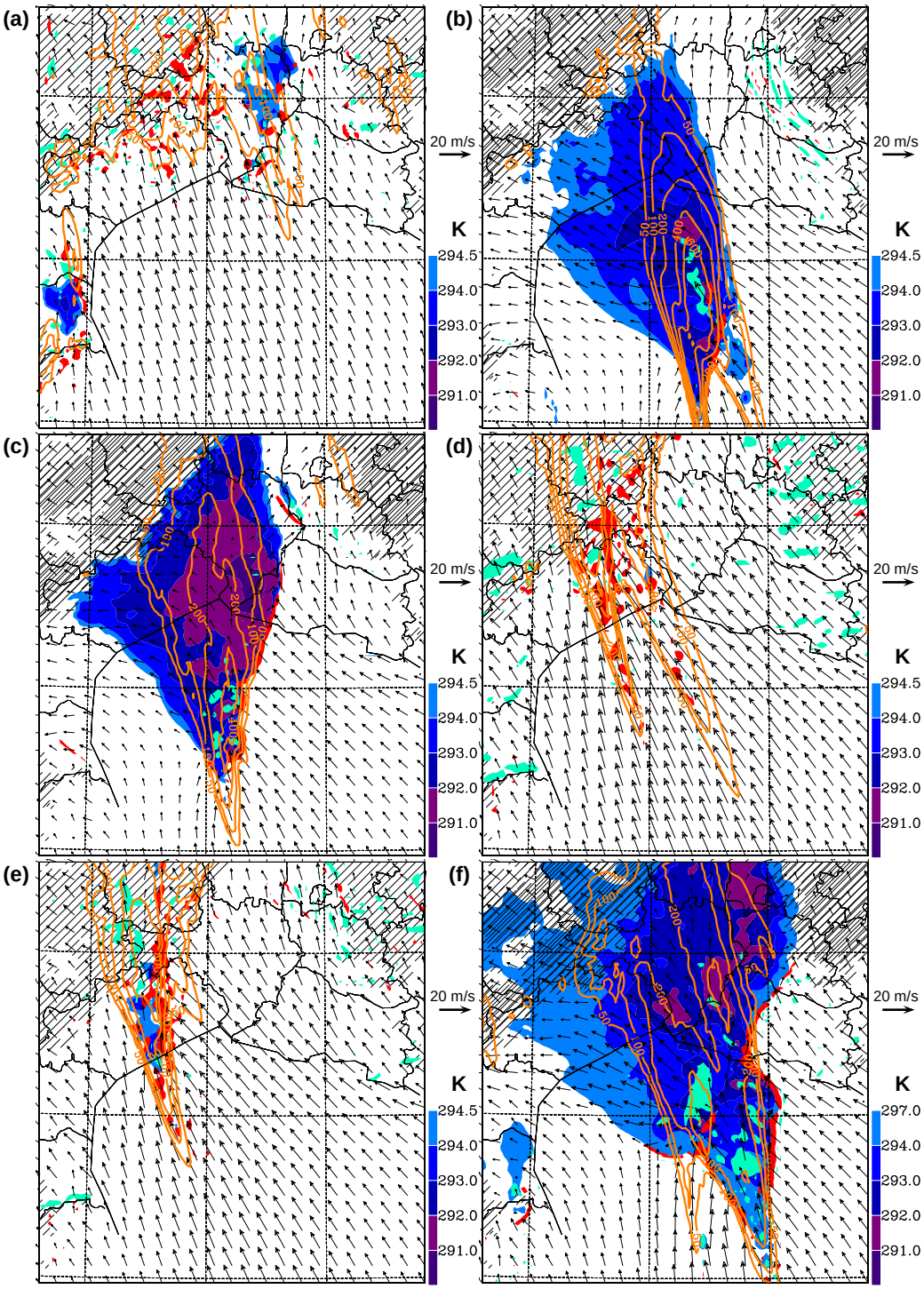

Figure 6: Same as Fig. 5b but for simulations UNIHU (a), STGHU (b), WIN10 (c), WIN20 (d), LCAPE (e), HCAPE (f).